International Journal of Solids and Structures 49 (2012) 111–120

Contents lists available at SciVerse ScienceDirect

International Journal of Solids and Structures

journal homepage: www.elsevier.com/locate/ijsolstr

Micromechanical stress–displacement model for rough interfaces: Effect of asperity contact orientation on closure and shear behavior

Anil Misra *, Shiping Huang

Department of Civil, Environmental and Architectural Engineering, The University of Kansas, United States

ARTICLE INFO

Article history:
Received 14 May 2011
Received in revised form 31 August 2011
Available online 24 September 2011

Keywords:
Rough contact
Stress–displacement relationship
Asperity orientation
Normal-shear coupling

ABSTRACT

The coupled normal-shear contact behavior of rough surfaces remains a problem of interest with applications in many practical engineering problems. In this paper, we have further developed a micromechanical approach for obtaining the stress–displacement behavior of rough interfaces. The micromechanical approach considers the mechanics of asperity contacts and utilizes statistical description of interface roughness. Here we have focused upon the role of asperity contact orientations. To that end, we have incorporated asperity contact relative curvature distribution in our model and derived a relationship for the extent of asperity contact orientations in terms of the asperity contact relative curvature and interface closure. This relationship allows us to define the range of asperity contact orientation as the interface is subjected to combined normal and shear loading. We have consequently refined our stress–displacement relationship and its numerical evaluation procedure to include the asperity contact relative curvature distributions. We find that the asperity contact relative curvature has a significant effect on the extent of asperity contact orientation, and consequently on the shear behavior of the interface. We also find that the coupling between the normal and the shear responses, the interface frictional strength and the shear displacement hardening behavior are closely related to the extent of asperity contact orientations.

1. Introduction

All surfaces are rough by nature irrespective of the scale of observation. The contact mechanics of interfaces formed by joining surfaces is, therefore, a fundamental problem in engineering. The understanding of the rough contact behavior and its effective modeling continues to be a challenging problem even with contributions spanning more than a century. The pioneering work related to the contact mechanics of deformable bodies is attributed to Hertz (1881, 1882) who developed the stress–displacement relationship of contact between two perfectly smooth convex elastic bodies under normal interfacial loading. Hertz's work was subsequently extended to a variety of loading conditions and material behavior, notable among which is the solution for the contact behavior of two smooth spheres under combined normal and shear loading by Mindlin and Deresiewicz (1953). Hertz–Mindlin solutions have provided the foundation of most developments in contact mechanics. However, since the middle of the 20th century, there has been an increasing realization that even the elastic contact behavior between real surfaces is much more complicated than that predicted by Hertz, Mindlin and other elasticity solutions. The root cause of this complexity, that has confounded the development of universal approaches for contact models, is the presence of numerous irregular asperities which strongly affect the contact behavior.

Numerous researchers have investigated approaches for incorporating the effect of asperity contacts. The notable early efforts along these lines can be traced to the works of Archard (1957), Bowden and Tabor (1950), Greenwood and Tripp (1971) and Greenwood and Williamson (1966). The recent approaches of rough contact modeling can be considered in three categories: (1) direct simulation using the finite element or equivalent method (Hyun et al., 2004; Laursen, 2002; Wriggers, 2006; Yoshioka, 1994), (2) fractal representation (Ciavarella et al., 2006; Hyun et al., 2004; Majumdar and Bhushan, 1990; Persson et al., 2005; Yang and Komvopoulos, 2005) and (3) statistical methods (Brown and Scholz, 1985; Buczkowski and Kleiber, 2009; Bush et al., 1975; Carbone, 2009; Greenwood, 2006; Greenwood and Williamson, 1966; Mccool and Gassel, 1981; Misra, 1997). Although direct simulation gives a detailed local behavior of asperity contact, it suffers from expensive computational expense and could even fail to converge due to the irregular geometry and local slip. Along the lines of fractal model, the scale dependent property of the rough surfaces is considered, however, the local behavior, especially sliding, is ignored in the fractal models. In contrast to the fractal model and

* Corresponding author. Address: Civil, Environmental and Architectural Engineering Department, The University of Kansas, Learned Hall, 1530 W. 15th Street, Lawrence, KS 66045-7609, United States. Tel.: +1 785 864 1750; fax: +1 785 864 5631.

E-mail address: amisra@ku.edu (A. Misra).

0020-7683/$ - see front matter © 2011 Elsevier Ltd. All rights reserved.
doi:10.1016/j.ijsolstr.2011.09.013

direct simulation, the statistical approach offers an efficient approach to describe the surfaces while incorporating the local asperity contact behavior and the potential scale-dependent property of surfaces. We note here that the number of references in each category are too numerous to include here so we have limited ourselves to cite a selection; the reader should be able to reconstruct the literature by following the references cited therein as well as in the recent reviews on the topic (Barber and Ciavarella, 2000; Zavarise and Paggi, 2008).

The interest in statistical methods has sustained since its introduction in 1960s and the approach of Greenwood and coworkers (referred to as the GW approach) has been widely applied. The GW approach considers that the asperity contacts form only at the summits, which represents the contact between a flat surface and a rough surface. However, for two rough surfaces, contact is possible at points other than the summit. Thus, the GW approach models the contact between two rough surfaces as equivalent to that between a flat surface and a rough surface. In recent years, the GW approach has been refined (Carbone, 2009; Greenwood, 2006) by using the rough surface analysis of Nayak (1971) which allows for the consideration of joint probability distributions of summit heights and curvatures. Within this approach, the scale-dependency of rough surfaces can be modeled by considering scale-dependent power spectral density functions (Zavarise and Paggi, 2008). An alternative statistical approach was developed by Brown and Scholz (1985) by considering the formation of contact between any two points of the rough surfaces. This alternative approach admitted the possibility of contacts that are inclined with respect to the nominal contact direction of the two rough surfaces. However, the effect of the tangential forces present at the inclined contacts was treated in an approximate manner. In an extension of this approach, the author (AM) had introduced an asperity contact orientation distribution and developed a stress–displacement model of rough interfaces under normal and shear loading (Misra, 1997) and applied it to model anisotropic interfaces (Misra, 1999), and surfaces undergoing damage (Misra, 2002). This extended model has shown that the asperity inclination has a significant effect on the tangential stiffness and friction behavior of the interfaces. More recently, we have utilized the approach to develop numerical implementation applicable for modeling rough contact behavior under combined normal and shear loading (Misra and Huang, 2009). It is noteworthy that most of the application of the statistical methods has been to closure behavior under loading in the normal direction to the nominal orientation of the interface. The applications of the statistical methods to the shear behavior as well as the coupled shear and normal behavior of rough interfaces have been relatively few (Archard, 1957; Buczkowski and Kleiber, 2009; Ford, 1993; Misra, 1997; Yoshioka and Scholz, 1989a).

The present work extends the statistical approach by (1) incorporating the asperity contact relative curvature distribution, (2) relating the asperity contact orientation range to the asperity contact relative curvature and interface closure, and (3) further extending the numerical implementation to solve the derived nonlinear stress–displacement equation system under mixed force and displacement loading conditions. We find that the asperity contact relative curvature distribution has a significant effect on the extent of asperity contact orientation, and consequently on the shear behavior of the interface. We also find that the coupling between the normal and the shear behavior, the interface frictional strength, and the shear displacement hardening behavior are closely related to the extent of asperity contact orientations.

In the subsequent discussion, we first briefly present our approach for statistical modeling of contact surface via asperity contact height, relative curvature and orientation distributions, and the connection between them. We then derive the nonlinear stress–displacement relationship for rough contact based on kinematically driven micromechanical methodology (Misra, 1997, 1999) and provide the numerical procedure utilizing Newton–Raphson method for evaluating the stress–displacement relationship. Finally, we validate our numerical results via comparison with experimental data for interface closure and shear under constant normal stress.

2. Statistical description of contact interface

The roughness of a surface may be considered in terms of statistics of parameters, such as heights, slopes and curvatures, which describe its deviation from a plane surface. Such statistical descriptions have been investigated first by Longuet-Higgins (1957a,b) and later by Nayak (1971) in the context of Gaussian rough surfaces. It was shown that while the surface heights and curvatures are statistically dependent, the slopes are statistically independent for random Gaussian surfaces. The joint probability distribution of heights and curvatures obtained from this analysis has been applied for modeling rough surface contact behavior assuming that the contact occurs only at the summits, such as that between a flat and a rough surface (Carbone, 2009; Greenwood, 2006).

However for two rough surfaces, the asperity contact can form between any two points of the surfaces. In this case, the relationship between surface topography measurements and the statistical descriptions of actual asperity contacts are far from clear. Nevertheless, the composite topography, obtained as the sum of the heights of the two surfaces (Brown and Scholz, 1985, 1986; Yoshioka and Scholz, 1989a) can be used to define the asperity contacts. As a first approximation, we assume that the asperity contact heights, curvatures and orientations for the composite topography are statistically independent. Given that the slopes of the individual surfaces are statistically independent of the heights and curvatures (Longuet-Higgins, 1957b), the assumption regarding the statistical independence of asperity contact orientation can be considered reasonable. In contrast, the statistical independence of asperity contact heights and curvatures is likely only under certain restrictive conditions and their joint probability distribution for composite topography requires further analysis. The motivation for the assumption of statistical independence is to simplify the analysis for combined normal and shear loading of the rough interface. In a future paper we will examine this assumption in a greater detail.

2.1. Asperity contact heights and curvatures

The asperity contact height, r, is determined with reference to the highest peak of this composite topography, such that the asperity contact height represents the overlap of the interacting surfaces. The probability density function of these asperity contact heights is bounded by zero and is likely to be skewed (Yoshioka and Scholz, 1989a,b). Such a probability density function can then be modeled as a gamma distribution, $H(r)$, given as:

$$H(r) = \frac{r^{\alpha}\exp(-r/\beta)}{\Gamma(\alpha+1)\beta^{\alpha}} \quad (0 < r < \infty,\ \alpha > -1,\ \beta > 0) \tag{1}$$

where α and β are parameters related to the mean and variance of the asperity contact heights as follows

$$\begin{aligned} &\textit{mean}: && r_m = (\alpha+1)\beta \\ &\textit{variance}: && r_\sigma^2 = (\alpha+1)\beta^2 \end{aligned} \tag{2}$$

Parameter α is unit less while parameter β takes the unit of asperity contact height. Surfaces that have smaller average asperity contact height and narrow distributions of asperity contact heights are considered to be smoother. Fig. 1 gives examples of asperity contact

height distributions for rough and smooth interfaces based upon the measurements reported in the literature. In Fig. 1(a), the measured height distributions for Westerly granite samples reported by Yoshioka and Scholz (1989a) are plotted along with the best-fit gamma distributions. In Fig. 1(b) the asperity contact height distribution for marble samples are plotted based upon the mean and the standard deviation of heights reported by Xia et al. (2003). For an interface with N asperities per unit area, $NH(r)\,dr$ denotes that number of asperity contacts in the interval represented by r and $r + dr$.

For an asperity contact, a relative radius of curvature, R, is defined according to the Hertz theory of normal contact between spherical elastic bodies as:

$$1/R = 1/R_1 + 1/R_2 \tag{3}$$

where R_1 and R_2 are the radii of curvatures of the two surfaces at an asperity contact. Taking $R_1 = eR_2$, where $R_2 > R_1$ so that $0 < e < 1$, asperity contact relative radius of curvature can be rewritten as:

$$R = R_1R_2/(R_1 + R_2) = \frac{e}{1+e}R_2 \tag{4}$$

The probability density function of the asperity contact relative curvature, denoted by $p(R)$, is modeled as a Gaussian distribution given below:

$$p(R) = \frac{1}{2\pi R_\sigma^2}\exp\left(-\frac{(R-R_m)^2}{2R_\sigma^2}\right) \tag{5}$$

where R_σ is the standard deviation and R_m is the mean of the asperity contact relative radii of curvature. Surfaces that have smaller mean and larger variance for asperity contact relative radii of curvatures are considered to be rougher, as shown Fig. 2. Since Gaussian distribution extends to minus infinity, for practical purposes the calculations are truncated to $\pm 3R_\sigma$.

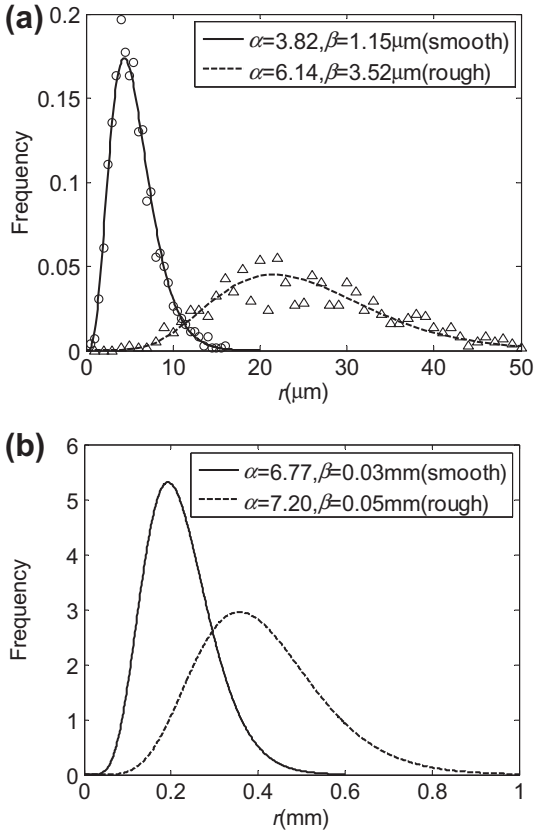

Fig. 1. Examples of asperity contact height distributions.

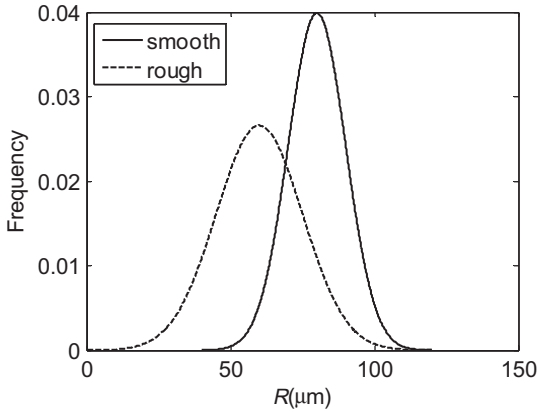

Fig. 2. Examples of asperity contact relative radii of curvatures distributions.

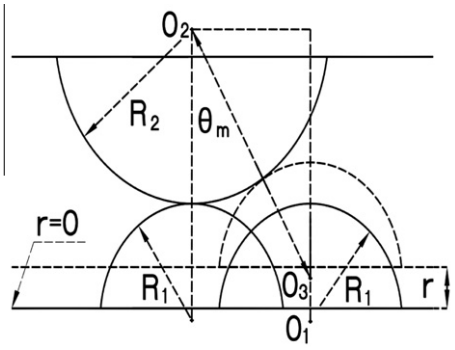

Fig. 3. Schematic depiction of the relationship between extent of asperity contact orientation, and radii of curvatures of interfaces 1 and 2.

2.2. Asperity contact orientations

The asperity contacts at rough interfaces can be inclined with respect to the nominal interface direction. Fig. 3 gives a schematic illustration of the relationship between asperity contact inclination, radii of curvatures and interface closure for the case that the incipient contact occurs at the asperity summits. For this case, we observe from the figure that at incipient interface contact all asperity contacts are in the 1-direction and the contact angle is zero. As the interface closure increases, new asperity contacts will form that are inclined to the first.direction. For the cases in which the initial contacts form at points other than the summits of the two surfaces, inclined asperity contacts will be present at the incipient contact. In either case, since the asperity heights, curvatures and relative locations are uncertain; the asperity contacts at the interfaces of rough surfaces take various orientations with respect to the nominal direction of the interface. We define the asperity contact orientation as the normal vector, $\mathbf{n}$, given in terms of the azimuthal angle, ϕ, and the meridional angle, θ, measured with respect to a Cartesian coordinate system in which direction 1 is normal to the nominal interface as shown in Fig. 4. We now consider the distribution density of contact orientation defined as

$$\xi(n_i) = \frac{1}{M}\sum_{j=1}^{M}\delta\left(n_i - n_i^j\right) \tag{6}$$

where, M is the total number of asperity contact, and $\delta(\boldsymbol{n} - \boldsymbol{n}^j) = \delta(\theta - \theta^j)\delta(\phi - \phi^j)/sin\theta^j$. Kanatani (1984) has shown that the

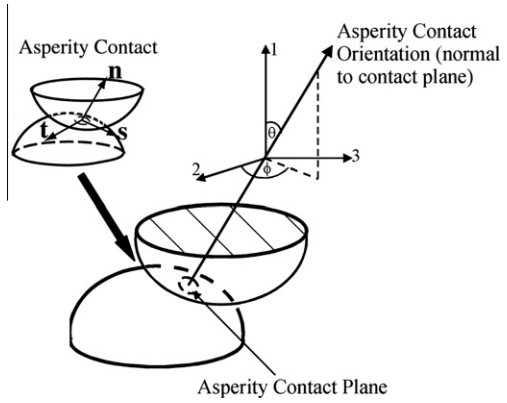

Fig. 4. Depiction of an asperity contact orientation with respect to a global coordinate system.

observed directional density of the type given by Eq. (6) can be estimated as smooth orientation distribution function of the form:

$$\xi(n_i) = \frac{1}{4\pi}[1 + \Phi_{ij} n_i n_j + \Phi_{ijkl} n_i n_j n_k n_l + \cdots] \tag{7}$$

where the nth rank tensors Φ are coefficient tensors such that the expansion is equivalent to the spherical harmonic expansion given as (see also Chang and Misra, 1990):

$$\xi(n_i) = \frac{1}{4\pi}\left\{1 + \sum_{k=2}^{\infty}{}' \left[a_{k0} P_k(\cos\theta) + \sum_{m=1}^{k} P_m^k(\cos\theta)(a_{km}\cos m\phi + b_{km}\sin m\phi)\right]\right\} \tag{8}$$

where $\sum'$ = summation over even indices, P_k = kth Legendre polynomial, P_k^m = the associated Legendre functions, and a_{k0}, a_{km} and b_{km} are the coefficients.

We note that the orientational density function given by Eqs. (7) and (8) are defined in a spherical domain. In contrast, the asperity contact orientation is bounded within a conical domain as depicted in Fig. 5 given by: $0 \leqslant \theta \leqslant \theta_m$, $0 \leqslant \phi \leqslant 2\pi$, where θ_m denotes the extent of asperity contact orientations in the meridional direction. From Fig. 3 we see that the relationship between asperity contact orientation extent, θ_m, and the relative radii of curvatures can be obtained as follows for a given interface closure, r:

$$\theta_m = \cos^{-1}\left(1 - \frac{r}{R_1 + R_2}\right) = \cos^{-1}\left(1 - \frac{e}{(1+e)^2}\frac{r}{R}\right) \tag{9}$$

where θ_m is the largest meridional angle, R is the relative radius of curvature, r is the closure and $e/(1+e)^2$ is the curvature modification factor which depends on the ratio R_1/R_2. Since θ_m can take the values in the range of 0 to $\pi/2$, we can write θ_m as $\pi/2a$, where parameter a takes the value from 1 to ∞. Thus the domain of asperity contact orientations becomes: $0 \leqslant \theta \leqslant \pi/2a$, $0 \leqslant \phi \leqslant 2\pi$, showing

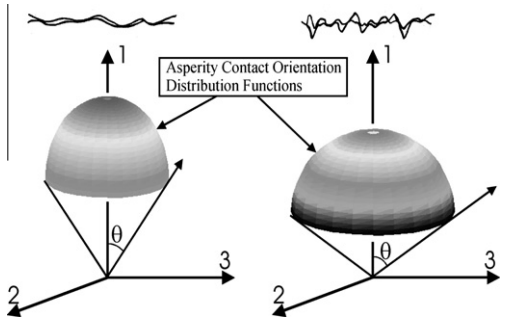

Fig. 5. Schematic depiction of asperity contact orientation distribution and its relationship to asperity contact heights and curvatures (Misra, 1997).

that the conical domain can be mapped onto a spherical domain by using a scaled or shifted meridional coordinate $a\theta$. In this case, the orientational density function given by Eqs. (7) and (8) can be applied to the conical domain by using shifted meridional coordinates as introduced by Misra (1997, 1999). The relationships between the largest meridional angle, θ_m, the asperity contact orientation parameter, a, and the ratio of the interface closure to the relative radius of curvature, r/R, are plotted in Fig. 6 for different e. The ratio r/R is related to the asperity contact height distribution and initial interface closure. For interfaces with the ratio r/R in the range of 0.1–1.0, the maximum asperity orientation will range from 15° to 45° with respect to the 1-direction. Further, we note that for highly mated surfaces with large initial closure, Eq. (9) will correctly result in large maximum asperity orientations. We also observe that the maximum asperity orientation decreases with the factor e, indicating that asperity contact orientations become small for surfaces with contrasting radii of curvatures. For $e = 0$, that is the contact of a flat surface with a rough surface, Eq. (9) correctly yields $\theta_m = 0$. On the other hand, for surfaces with similar radii of curvatures, that is for factor e in the range 0.5–1, there is minimal effect on the maximum asperity orientation.

For practical calculations, we consider only terms with $k = 2$ in Eq. (8) to obtain a simple truncated form of the shifted spherical harmonic expansion as:

$$\xi(\Omega) = \frac{1}{2\pi}\left[1 + \frac{b}{4}(3\cos a\theta + 1) + 3\sin^2 a\theta(c\cos 2\phi + d\sin 2\phi)\right] \quad \text{for } \left(0 \leqslant \theta \leqslant \frac{\pi}{2a}; 0 \leqslant \phi \leqslant 2\pi\right) \tag{10}$$

where angles ϕ and θ are defined in Fig. 4, Ω represents the solid angle formed by ϕ and θ, and parameters a, b, c and d determine

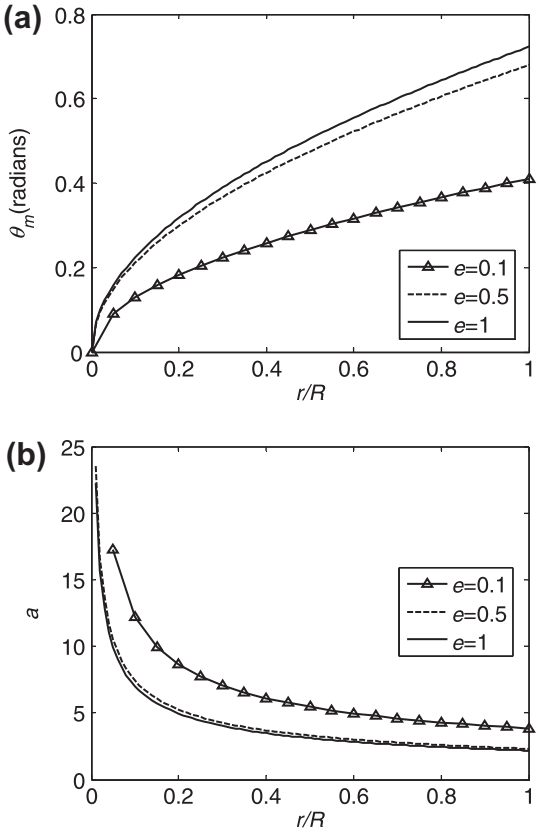

Fig. 6. (a) θ_m versus r/R and (b) parameter a versus r/R.

the shape of the density function $\xi(\Omega)$. It is straightforward to show that:

$$\int_0^{2\pi}\int_0^{\pi/2a}\xi(\Omega)a\sin a\theta d\theta d\phi = 1 \tag{11}$$

The density function in Eq. (10) has the ability to model surfaces of varying roughness. As discussed in Misra (1999), more asperity contacts orient in the direction perpendicular to the interface for smooth surfaces than that for rough surfaces. Accordingly, for a given e, as parameter, a, increases or r/R decreases (as shown in Fig. 6(b)), the contact distribution concentrates toward the direction normal to the interface (along the 1-axis of the global Cartesian coordinate system in Fig. 4). In particular, the density function, $\xi(\Omega)$, behaves like a delta function in the limit $a \to \infty$ or $r/R \to 0$ yielding an expectation $E[\theta] = 0$, which represents a concentrated contact orientation, normal to a perfectly smooth interface. While parameter, a, describes the extent of the asperity contact orientations, parameter, b, determines the shape of the orientation distribution in the meridional direction, θ. With different combinations of parameters a, and b, the density function of asperity contact orientations can represent interfaces with varying anisotropy in the meridional direction as illustrated in Fig. 7. For isotropic distribution of orientations in the meridional direction, the parameter, b, is a function of the parameter, a, and the orientation angle, θ. Parameter, c and d, determine the shape of the orientation distribution in the azimuthal direction, ϕ. For isotropic surfaces, parameters, c and d, take the value zero. In Fig. 8 we show how the asperity contact orientations probability density varies with parameter, a, and θ_m for isotropic interfaces.

3. Micromechanical stress–displacement Relationship

Stress–displacement relationship is based upon the kinematically driven micromechanical approach described previously.

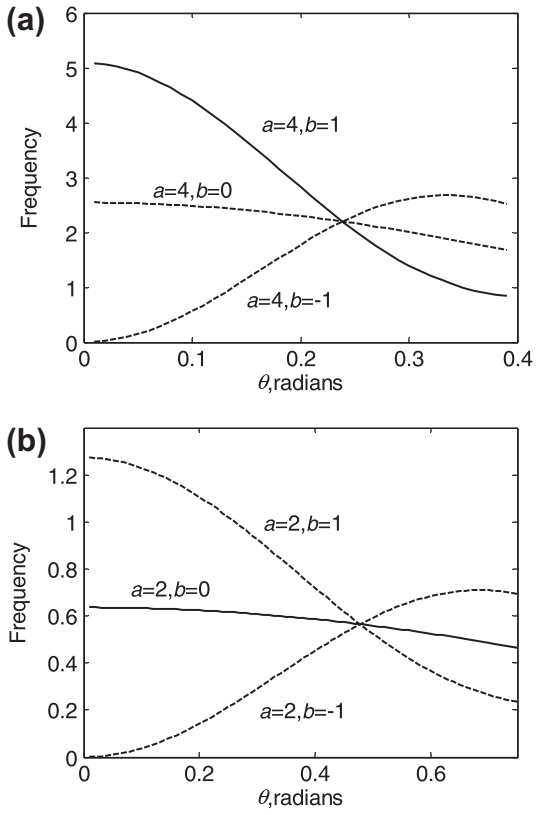

Fig. 7. Asperity contact orientation distributions for different parameters.

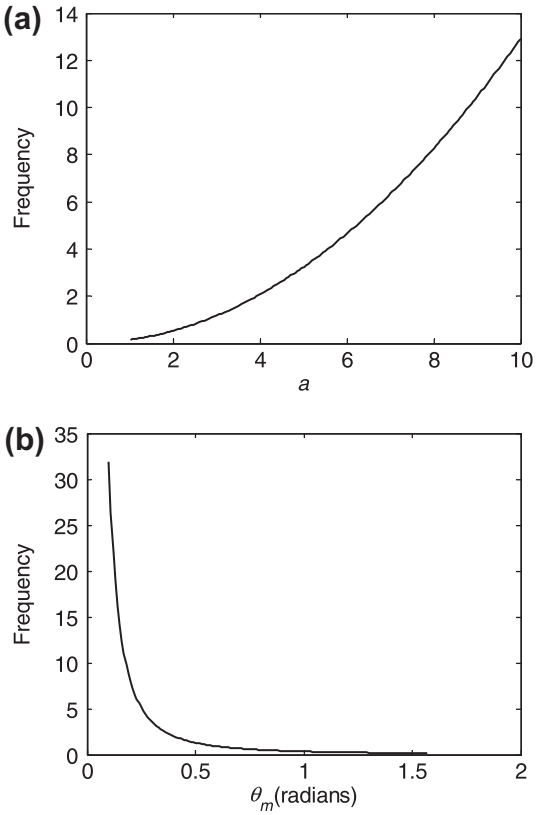

Fig. 8. Asperity contact orientation density for isotropic interface (a) as a function of parameter, a, and (b) as function of θ_m.

(Misra and Huang, 2009). For completeness, we present here a brief description of the model derivation.

3.1. Asperity contact displacement

In the kinematically driven approach, we assume that the asperity displacement, δ_j, at a given asperity contact height is the same and directly related to the overall displacement of the interface, Δ_j. This kinematic assumption disregards the nonlocality of asperity contact interactions. The assumption is reasonable for interfaces with relatively large asperity spacing in stiff materials such that the overlap of deformation fields associated with neighboring asperity contacts is minimal and the statistical description of the interface remains unchanged during loading. This assumption has been widely used and appears to be especially useful for describing contacts between metals and stiff geo materials. In this case, the asperity displacements are written in terms of the overall interface displacements as follows:

$$\begin{Bmatrix}\delta_n\\ \delta_s\\ \delta_t\end{Bmatrix} = \begin{bmatrix}n_1 & n_2 & n_3\\ s_1 & s_2 & s_3\\ t_1 & t_2 & t_3\end{bmatrix}\begin{Bmatrix}\Delta_1 - r\\ \Delta_2\\ \Delta_3\end{Bmatrix} \tag{12}$$

where δ_n is the asperity normal displacement, while δ_s and δ_t are the asperity shear displacements resolved along the local coordinate axes. The local Cartesian coordinate system is formed by the normal vector, **n**, shown in Fig. 4, and vectors, **s** and **t** chosen arbitrarily on the plane tangential to the asperity contact surface, such that the vectors **nst** are given as follows:

$$\begin{aligned} n_i &= \langle \cos\theta,\ \sin\theta\cos\phi,\ \sin\theta\sin\phi\rangle\\ s_i &= \langle -\sin\theta,\ \cos\theta\cos\phi,\ \cos\theta\sin\phi\rangle\\ t_i &= \langle 0,\ -\sin\theta,\ \cos\phi\rangle \end{aligned} \tag{13}$$

The subscripts in this paper follow the established tensor convention unless specified otherwise.

3.2. Asperity contact force

The relationship between the asperity contact forces, f_i, and displacements, Δ_j, is then defined as follows:

$$f_i = K_{ij}(\Delta_j - \delta_{1j}r) \tag{14}$$

where the asperity contact stiffness tensor, K_{ij}, given by:

$$K_{ij} = K_n n_i n_j + K_{st}(s_i s_j + t_i t_j) \tag{15}$$

where K_n and K_{st} denote asperity stiffness along the normal and tangential directions of the asperity contact. The coupling between the normal and shear behavior at the asperity-level is considered to be negligible. The asperity contact stiffnesses are obtained from the Hertz–Mindlin contact theory of perfectly smooth elastic interfaces (Johnson, 1985). The asperity contact normal stiffness is given as:

$$f_n = K_n\delta_n = \lambda K\delta_n^{\eta+1} \tag{16}$$

where, f_n is the contact normal force, and K, λ and η are constants, which take the values:

$$\lambda = \frac{2-\nu}{2(1-\nu)}; \quad \eta = \frac{1}{2}; \quad K = \frac{8G\sqrt{R}}{3(2-\nu)} \tag{17}$$

where G is the material shear modulus, ν is Poisson's ratio and R is relative radius of curvature.

The asperity contact loading in the tangential direction is complicated when an interface is subjected to a sequential loading in which an interface is first subjected to a normal closure followed by shearing as is typically done in laboratory experiments. In this case, the inclined asperity contacts first experience tangential loading along specific directions (determined by their orientations) as the interface is subjected to normal closure. Subsequently, the asperity contact experiences out-of-plane tangential loading, such as that denoted by T_2 in Fig. 9(a), where the N–T plane represents the asperity contact loading condition under normal closure. It is noteworthy that the widely cited solutions given by Mindlin (1949) and Mindlin and Deresiewicz (1953) only consider contact loading confined within an N–T plane. For loading confined in an N–T plane, a contact can be considered to be undergoing either loading or unloading. However, when the shear forces are out-of-plane, both loading and unloading can happen simultaneously in orthogonal shear directions. As a result additional energy is expended in undergoing this loading–unloading–reloading loop and the resultant tangential displacements and force are likely to be non-coaxial. In Fig. 9(b) we show as an example calculation for the case in which we first apply on an asperity a tangential force T_1 in a given direction and then apply T_2 such that the angle between T_1 and T_2 is $2\pi/3$. Upon the application of force T_1, the tangential force displacement curve follows the path 0–A as shown in Fig. 9(b). Subsequently, upon the application of force T_2, the contact first experiences unloading from A to B as the resultant tangential force decreases. As T_2 is increased further, the resultant tangential force begins to increase and the contact again experiences loading from B to A to C. The consequent hysteretic loop represents a loss of energy during this loading process. The size of the loop is determined by the angle between T_1 and T_2. To our knowledge, solutions for cases that involve varying shear directions do not exist, however, models based upon 2-d plasticity have been proposed (Dobry et al., 1991) and applied to rough contact modeling (Buczkowski and Kleiber, 2009). The complete loading history of each asperity contact must be strictly followed to determine the true tangential traction, slip annulus and the resultant tangential force–displacement behavior as illustrated in Fig. 9(b). Clearly,

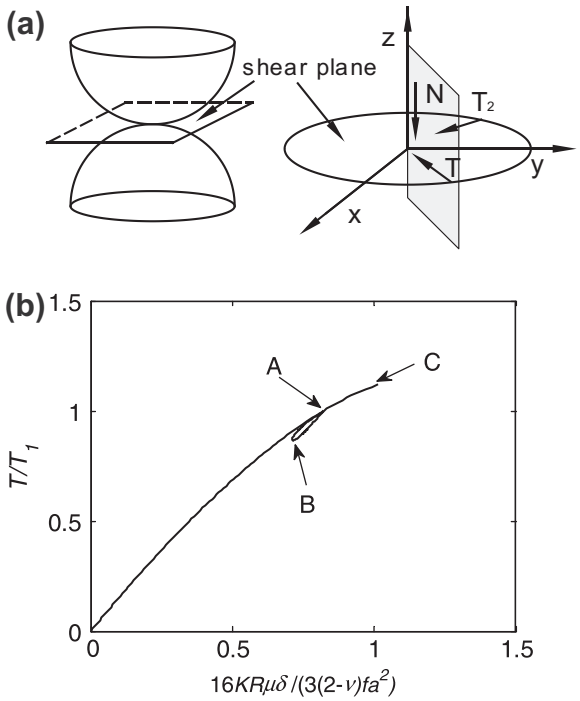

Fig. 9. (a) Schematic of arbitrarily directed asperity contact shear loading, and (b) resultant tangential force–displacement curve.

such an approach will entail additional computational efforts. For the case of monotonic shear loading subsequent to normal loading considered in this paper, the effect of unloading at individual asperity are expected to be small, since in this case only one directional change is involved. Therefore, for our calculations we have considered the case of constant normal asperity force and monotonically increasing asperity shear force, such that the asperity shear force–displacement relationship is given as:

$$f_s = \mu K_n\delta_n\left[1-\left(1-\frac{\delta_{st}}{\lambda\mu\delta_n}\right)^{\frac{3}{2}}\right]\frac{\delta_s}{\delta_{st}} = K_{st}^{el}\delta_s \tag{18}$$

$$f_t = \mu K_n\delta_n\left[1-\left(1-\frac{\delta_{st}}{\lambda\mu\delta_n}\right)^{\frac{3}{2}}\right]\frac{\delta_t}{\delta_{st}} = K_{st}^{el}\delta_t \tag{19}$$

where K_{st} is the stiffness in the tangential direction, and the superscript *el* denotes asperity contacts that are not sliding. We note Eqs. (18) and (19) are valid when $|\lambda\mu\delta_n| > \delta_{st}$. When this condition is violated, sliding occurs at the contact per the Amonton–Coulomb's friction law. In this case Eqs. (18) and (19) can be rewritten as:

$$f_s = \mu K_n\delta_n\frac{\delta_s}{\delta_{st}} = K_{st}^{p}\delta_s \tag{20}$$

$$f_t = \mu K_n\delta_n\frac{\delta_t}{\delta_{st}} = K_{st}^{p}\delta_t \tag{21}$$

where the superscript p denotes asperity contacts that are sliding. In Eq. (18) through (21) the ratios δ_s/δ_{st} and δ_t/δ_{st} give the projection of the asperity contact shear force, f_{st}, in the s- and the t-directions, the stiffness, K_{st}, has been introduced for convenience, and δ_{st} is defined as the asperity shear displacement given by,

$$\delta_{st} = \sqrt{\delta_s^2 + \delta_t^2} \tag{22}$$

3.3. Interface stress–displacement relationship

Under a given loading, numerous asperity contacts occur at varying asperity contact heights, relative curvatures and orientations.

These asperity contacts can be classified into three groups: (1) those in contact but without sliding ($\lambda\mu\delta_n > \delta_{st}$), (2) those in contact but with sliding, and (3) those not in contact. The overall interface stress can be obtained as the sum of the asperity contact forces contributed by groups (1) and (2). Utilizing the orientation, relative curvature and height distributions introduced in Section 2, we obtain the following expression for the overall interface stress:

$$F_i = N\left(\int_{r^{el}}\int_{R^{el}}\int_{\Omega^{el}} f_i^{el}\xi(\Omega)d\Omega H(r)drp(R)dR + \int_{r^p}\int_{R^p}\int_{\Omega^p} f_i^{p}\xi(\Omega)d\Omega H(r)drp(R)dR\right) \quad (23)$$

Eq. (23) reduces to the composite topography models presented by (Brown and Scholz, 1985; Yoshioka and Scholz, 1989a) under their assumptions regarding the effect of asperity contact orientations. Furthermore, by eliminating the integration over the orientations such that only summit contacts are considered and introducing appropriate height and curvature distributions in Eq. (23), we can recover the GW model and its recent modifications for the normal closure of a rough surface in contact with a flat (Carbone, 2009; Greenwood, 2006).

Very often, we have to solve the nonlinear equation system given by Eq. (23) to obtain the displacements corresponding to the applied stress loading conditions or mixed loading conditions. In this paper, we utilize the Newton–Raphson method to solve this set of nonlinear equations. We define a residual force vector, $R_i(\Delta_i)$ as

$$R_i(\Delta_i) \equiv N\left(\int_{r^{el}}\int_{R^{el}}\int_{\Omega^{el}} f_i^{el}\xi(\Omega)d\Omega H(r)drp(R)dR + \int_{r^p}\int_{R^p}\int_{\Omega^p} f_i^{p}\xi(\Omega)d\Omega H(r)drp(R)dR\right) - F_i^E = 0 \quad (24)$$

where F_i^E is the external force vector. We expand the residual $R_i(\Delta_i)$ in Taylor's series with respect to displacement vector Δ_i at $(n-1)$th iteration to obtain:

$$R_j(\Delta_i) = R_j(\Delta_i)^{n-1} + \left(\frac{\partial R_j}{\partial \Delta_i}\right)^{n-1} d\Delta_i + \cdots \quad (25)$$

where we omit the terms of order 2 and higher. We can thus obtain the increment of displacement, $d\Delta_i$, corresponding to the residual at the $(n-1)$th iteration as

$$d\Delta_i = \frac{-R_j(\Delta_i)^{n-1}}{(T_{ji})^{n-1}} \quad (26)$$

where T_{ji} is defined as the tangent stiffness tensor given by,

$$(T_{ji})^{n-1} = \left(\frac{\partial R_j}{\partial \Delta_i}\right)^{n-1} \quad (27)$$

We subsequently update the interface displacement in the usual manner

$$(\Delta_i)^n = (\Delta_i)^{n-1} + d\Delta_i \quad (28)$$

The above numerical scheme has been implemented in the following 5-steps:

Step 1: Discretize the integration domain in Eq. (23) into sufficient integration points representing asperity contact heights, relative radii of curvatures and orientations so as to obtain a converged solution. Each integration point represents an asperity contact. For our computations we have used $\Delta r = 0.01 r_{90}$, where r_{90} = is the 90th percentile of asperity contact height for r-discretization, $\Delta R = 0.01 R_\sigma$, where R_σ, is standard deviation of the asperity contact relative radii of curvatures, and grid of 20×40 for θ and ϕ-discretization. It is noteworthy that for each loading step, θ_m is and a are changing according to Eq. (9). The integration is performed using Simpson's rule.

Step 2: Use the $(n-1)$th iteration displacement $(\Delta_i)^{n-1}$ to determine the asperity contact displacement using Eq. (12).

Step 3: Determine the sliding condition of each asperity and the contact force using Eq. (18) through (21). Sum all asperity contact forces to obtain the overall force, $(F_i)^{n-1}$, using discretized equation (23) as described in Step 1.

Step 4: Use a small interface displacement increment, $\partial\Delta_i$, typically taken as $0.01 r_{90}$, to obtain the asperity contact displacement increment and, consequently, the asperity contact force increment. Sum all asperity contact force increments to compute the corresponding increment of interface force, ∂F_j, and evaluate tangent stiffness using Eq. (27).

Step 5: Calculate the residual force $R_j^{n-1} = F_j^E - (F_j)^{n-1}$, and use Eq. (26) to find the interface displacement increment, $d\Delta_i$. Update the interface displacement $(\Delta_i)^n$ and check for convergence.

4. Results and discussion

We demonstrate the applicability of the derived overall stress–displacement relationship and its numerical implementation under combined normal-shear loading conditions. In the subsequent discussion, we first utilize a 3-step loading path to study the coupling behavior between normal and tangential loading. We then compare our numerical results with experimental data culled from literatures to verify our model.

4.1. Coupling effect between normal and tangential loading

According to the Hertz theory, for the contact of bodies with the same elastic constants, the normal force distribution is independent of the shear force. It is also shown by Johnson (Johnson, 1985), that even for dissimilar solids, the influence of tangential tractions upon the normal pressure and the contact area is quite small. However, for rough interface, the interaction of normal and tangential loading is significant. To this end, we have investigated the coupling effect between normal and tangential loading under a 3-step loading path for two interfaces with different roughness (R1 and S1). The input parameters for the interfaces R1 and S1 are as shown in Table 1. These parameters are for illustrative purpose and are based upon the work done by Yoshioka and Scholz (1989b). We assume that the initial closure is zero such that at the incipient interface contact, all asperity contacts are in the 1-direction, that is the asperity contact orientation is identically zero. The 3-step loading path is as follows (see Fig. 10): in step 1,

Table 1
Interface properties.

Parameters	*R1* (rough)	*S1* (smooth)	*R2* (rough)	*S2* (smooth)
Asperity density, N	200/mm^2	200/mm^2	0.2240/mm^2	0.2034/mm^2
R_m	50 μm	75 μm	8.82 mm	8.18 mm
R_σ	15 μm	10 μm	0.30 mm	0.20 mm
Asperity friction, μ	1	1	1	1
Shear modulus, G	80.0 GPa	80.0 GPa	31.8 GPa	31.8 GPa
Poisson's ratio, ν	0.3	0.3	0.152	0.152
Initial closure, r_o	0	0	0.10 mm	0.12 mm
Height distribution	α = 6.14 β = 3.52 μm	α = 3.82 β = 1.15 μm	α = 7.20 β = 0.05 mm	α = 6.77 β = 0.03 mm

we incrementally apply normal displacement (Δ_1) till a closure of 15 μm for rough interface and 6 μm for smooth interface; in step 2, keeping the interface closure the same as that at the end of step 1, we incrementally apply tangential displacement (Δ_2) till a shear displacement of 15 μm and 6 μm for the rough and smooth interfaces, respectively; finally in step 3, keeping the interface closure and shear displacements the same as at the end of step 2, we incrementally apply tangential displacement (Δ_3) till a shear displacement 15 μm and 6 μm for the rough and smooth interfaces, respectively. The results are shown in Fig. 11(a) and (b) for rough and smooth interfaces, respectively. We observe during the normal closure (step 1) that the orientation extent at the same normal stress is larger for the rough interface than the smooth interface. For rough interface, we observe that after step 1, the normal stress (F_1) changes significantly in steps 2 and 3 as tangential displacement increases. However, for the smooth interface, the normal stress changes insignificantly under the same condition. Thus the coupling effect between normal and tangential loading for rough contacting interfaces is much stronger compared to smooth contacting interfaces. In particular, if the contacting surfaces become perfectly smooth, there is no coupling between tangential traction and normal stresses. We also observe in step 2 that the tangential traction for smooth interface reaches an asymptote suggesting that it has achieved its frictional strength, while the tangential traction for the rough interface exhibits a displacement-hardening type behavior. We remark that the tangential traction of the interface has two contributions: one from the asperity normal force, and the other from the asperity tangential force which is proportional to the asperity normal force via the asperity friction coefficient. For rough interface, the asperity contact orientations are closer to the horizon, thus they can develop considerable normal forces. As a result the interface tangential traction shows a hardening trend and can achieve values greater than the interface normal stress. Finally, the validity of our numerical procedure is verified as the two tangential tractions become identical at the end of step 3 when the tangential displacements in 2- and 3-directions become the same. Such a result is expected for isotropic interfaces, whose surfaces do not experience wear and the geometry remains unchanged during the loading process.

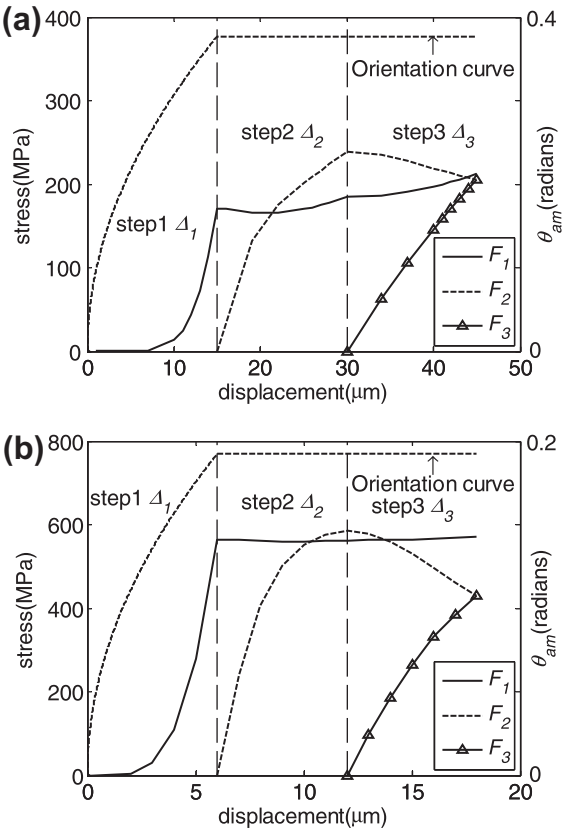

Fig. 11. Stress–displacement behavior under 3-step loading path: (a) rough interface, and (b) smooth interface.

4.2. Comparison of model prediction with measurements

In order to validate our model, we compared our numerical results to the experimental data culled from the literature. For the normal loading, the experimental data is based on the measurement on marble reported by (Xia et al., 2003). The model parameters are given in Table 1 for rough (R2) and smooth (S2) interfaces, respectively. This data correspond to the interfaces labeled MG21 and MG23 in the paper by Xia et al. The initial closure, r_o, for our calculation was taken such that the percent of impending asperity contacts was approximately 30% of the possible contacts. It can be seen in Fig. 12(a), the numerical results agree well with the experimental data. As expected, the smooth interface has larger stiffness than the rough interface. In Fig. 12(b) we show the evolution of asperity contact orientation extent with loading plotted in terms of the average asperity contact orientation extent, θ_{am}, defined as follows:

$$\theta_{am} = \int_R \cos^{-1}\left(1 - \frac{e}{(1+e)^2}\frac{r}{R}\right) p(R)dR \tag{29}$$

We note that for a given displacement the asperity orientation extents are almost identical, while the normal stresses are significantly different for the two interfaces. The stiff behavior of the smooth interface is, therefore, the result of higher number of contacts. Clearly, in this case, the asperity orientation extent has little effect on the normal stress–displacement behavior.

For the evaluation of shear behavior prediction, we have computed the result for the rough interface R1 and the smooth interface S1. The calculation is performed under mixed loading condition consisting of two steps. In step 1, we incrementally increase the normal stress to 500 MPa. In step 2, we keep the normal stress constant at 500 MPa and incrementally increase the tangential displacement till a substantial number of asperity contacts achieve sliding and the interface can be considered as failed in shear. The results of the step 2 loading are plotted in Fig. 13.

Fig. 13(a) shows the evolution of shear resistance, defined as the ratio of the interface shear and normal stresses, with shear displacement for smooth and rough interfaces. In Fig. 13(a) inset, we have included the measurements reported by Biegel et al.

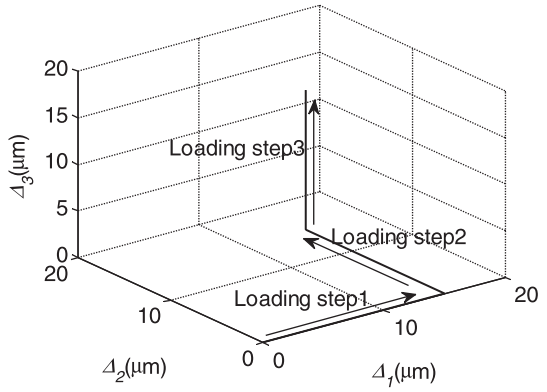

Fig. 10. The 3-step normal-shear loading procedure.

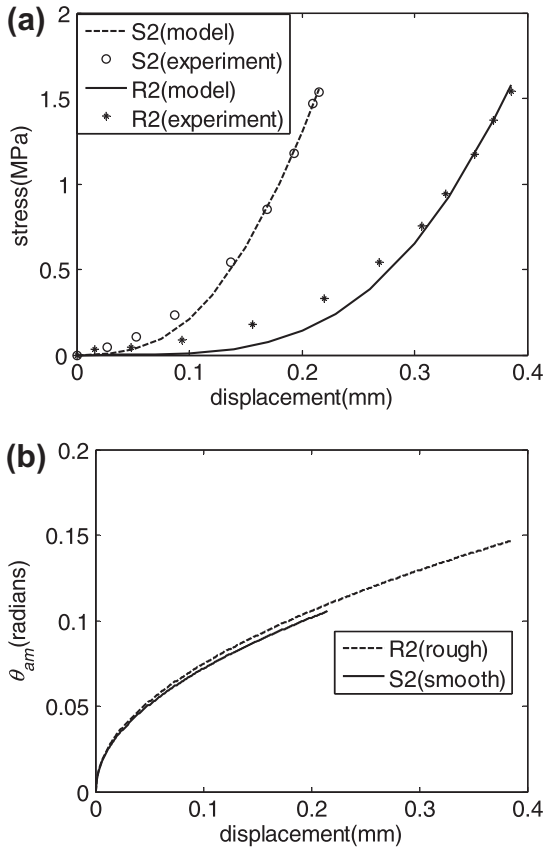

Fig. 12. (a) Comparison of the model result and experimental data under normal loading, and (b) the evolution of orientation extent for rough and smooth interfaces.

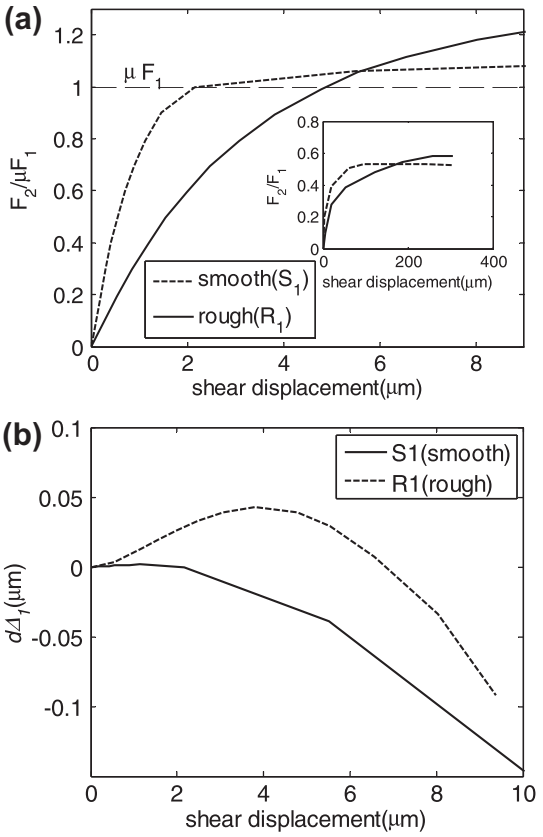

Fig. 13. (a) Shear resistance-displacement behavior and (b) closure behavior during interface shear under constant normal stress. The inset in (a) gives the measured results re-plotted from Fig. 11a of (Biegel et al., 1992).

(1992) on interfaces between two smooth or two rough surfaces of Westerly granite blocks. The computed results show qualitative agreement with the measurements. No attempt was made to obtain quantitative agreement due to lack of data for surface roughness parameters.

The difference between the shear behaviors of the smooth and rough interfaces in Fig. 13(a) may be considered in two distinct regimes of shear displacements. In the small shear displacement regime, we observe that the smooth interface is significantly stiffer in shear compared to the rough interface. Measurements performed on interfaces of similar materials but with different degrees of roughness (Biegel et al., 1992; Yoshioka and Scholz, 1989a) confirm that smoother interfaces are stiffer. The stiffer shear response of the smooth interface can be attributed to the concentration of asperity contact orientation distribution toward the direction normal to the interface. Under small shear displacements, the effect of applied normal stress is dominant. Therefore, interfaces with larger number of asperity contact in the direction normal to the interface or with a larger real contact area tend to be stiffer. At the large shear displacement regime, we observe that the curves crossover and the rough interfaces are found to have a higher shear resistance, and eventually, a higher frictional strength compared to smooth interfaces.

As the shear loading is increased, a larger proportion of asperity contacts inclined close to the direction normal to the interface begin to slide. Since smooth interfaces have a larger proportion of asperity contacts inclined close to the interface normal direction, the interface exhibits a rather sharp yield point with very little displacement hardening. As seen from Fig. 13(a), smooth interface reaches a frictional resistance only slightly greater than the asperity friction coefficient of 1. In contrast, the rough interface exhibits considerable displacement hardening without a distinct yield point and posses a significantly higher frictional resistance than the asperity friction coefficient. Since the extent of the asperity orientations depends upon the interface normal stress or closure as seen from Fig. 12(b), the proposed method will predict a nonlinear dependence of frictional resistance upon the interface normal stress for elastic asperity behavior.

The shear behavior is also affected by the strong coupling between normal and shear displacements. In Fig. 13(b) the closure behavior during interface shear loading is plotted as the normal displacement in step 2 of loading, $d\Delta_1$, versus Δ_2. Both interfaces first compress before dilating, with the rough interface experiencing greater compression as well as dilation compared to the smooth interface. Although the magnitude of normal displacement is small, it has significant effect upon the displacement hardening and frictional strength of interface.

5. Concluding remarks

The effect of asperity contact orientations on the stress–displacement behavior of rough interfaces has not been adequately investigated. Models based upon the composite topography approach, either ignore the asperity contact orientation or treat their effects in an approximate manner. As a consequence, these approaches have difficulty in describing a number of phenomena observed during interface shear, such as dilation-contraction and shear displacement hardening. In this paper, we have utilized a micromechanical model of rough interfaces to study the role of asperity contact orientations. This micromechanical model is based upon a methodology developed by the authors that considers

asperity contacts and statistical description of interface roughness (Misra, 1997, 1999; Misra and Huang, 2009). In the present approach, the asperity contact orientations are explicitly considered. In addition, we have extended our micromechanical model by incorporating the asperity contact relative curvatures distribution, and developing a relationship between the asperity contact orientation extent, relative curvature and interface closure. The nonlinear stress–displacement equation system of the extended model is solved by the Newton–Raphson method for different loading conditions. We demonstrate the applicability of the derived model under a variety of loading conditions for smooth and rough interfaces, including comparisons with experimental results.

The numerical results demonstrate that the model replicates the closure and shear behavior of smooth and rough surfaces both qualitatively and quantitatively. We find that the asperity contact relative curvature has a significant effect on the extent of asperity contact orientation. The relationship between interface closure and asperity orientation allows us to compute the evolution of the asperity contact orientation extent as the interface is subjected to normal loading. We find that the rough interfaces generally have a larger asperity orientation extent than the smooth interfaces. The orientation extent plays a significant role when the interface is sheared following the application of normal loading. We also find that the coupling between the normal and the shear response, the interface frictional strength and the shear displacement hardening behavior are closely related to the extent of asperity orientations.

Finally we observe that the shear behavior of the interfaces under constant normal stress should be considered in two distinct regimes of shear displacements. In the small shear displacement regime, the smooth interfaces are stiffer in shear compared to the rough interfaces. As the shear displacement is increased and a large number of asperity contacts reach their frictional resistance, the shear stress–displacements curves of the smooth and rough interfaces crossover. Thus, at the large shear displacement regime, the rough interfaces are found to have a higher shear resistance, and eventually, a higher frictional strength compared to smooth interfaces. While the smooth interfaces show an abrupt yield close to frictional strength, the rough interfaces exhibit a shear displacement hardening and gradual transition to frictional strength. This distinction in shear behavior with varying roughness can also be attributed to the extent of asperity contact orientations.

References

Archard, J.F., 1957. Elastic deformation and the laws of friction. Proceedings of the Royal Society of London Series A-Mathematical and Physical Sciences 243, 190–205.

Barber, J.R., Ciavarella, M., 2000. Contact mechanics. International Journal of Solids and Structures 37, 29–43.

Biegel, R.L., Wang, W., Scholz, C.H., Boitnott, G.N., Yoshioka, N., 1992. Micromechanics of rock friction, 1, Effects of surface roughness of initial friction and slip hardening in Westerly Granite. Journal of Geophysical Research-Solid Earth 97, 8951–8964.

Bowden, F.P., Tabor, D., 1950. The Friction and Lubrication of Solids. Oxford, Clarendon, United Kingdom.

Brown, S.R., Scholz, C.H., 1985. Closure of random elastic surfaces in contact. Journal of Geophysical Research-Solid Earth and Planets 90, 5531–5545.

Brown, S.R., Scholz, C.H., 1986. Closure of rock joints. Journal of Geophysical Research-Solid Earth and Planets 91, 4939–4948.

Buczkowski, R., Kleiber, M., 2009. Statistical models of rough surfaces for finite element 3D-contact analysis. Archives of Computational Methods in Engineering 16, 399–424.

Bush, A.W., Gibson, R.D., Thomas, T.R., 1975. Elastic contact of a rough surface. Wear 35, 87–111.

Carbone, G., 2009. A slightly corrected Greenwood and Williamson model predicts asymptotic linearity between contact area and load. Journal of the Mechanics and Physics of Solids 57, 1093–1102.

Chang, C.S., Misra, A., 1990. Packing structure and mechanical-properties of granulates. Journal of Engineering Mechanics-Asce 116, 1077–1093.

Ciavarella, M., Delfine, V., Demelio, V., 2006. A new 2D asperity model with interaction for studying the contact of multiscale rough random profiles. Wear 261, 556–567.

Dobry, R., Ng, T.T., Petrakis, E., Seridi, A., 1991. General-model for contact law between two rough spheres. Journal of Engineering Mechanics-Asce 117, 1365–1381.

Ford, I.J., 1993. Roughness effect on friction for multi-asperity contact between surfaces. Journal of Physics D-Applied Physics 26, 2219–2225.

Greenwood, J.A., 2006. A simplified elliptic model of rough surface contact. Wear 261, 191–200.

Greenwood, J.A., Tripp, J.H., 1971. The contact of two nominally flat rough surfaces. Proceedings of the Institution of Mechanical Engineers 185, 625–633.

Greenwood, J.A., Williamson, J.B., 1966. Contact of nominally flat surfaces. Proceedings of the Royal Society of London Series A-Mathematical and Physical Sciences 295, 300–319.

Hertz, H., 1881. On the contact of elastic solids. Journal fur de reine und angewandte Mathematik 92, 156–171.

Hertz, H., 1882. On the contact of rigid elastic solids and on hardness. Verhandlungen des Vereins zur Befoderung des Gewerbefleisses.

Hyun, S., Pei, L., Molinari, J.F., Robbins, M.O., 2004. Finite-element analysis of contact between elastic self-affine surfaces. Physical Review E 70, 026117-026111-026112.

Johnson, K.L., 1985. Contact Mechanics. Cambridge University Press, Cambridge, UK.

Kanatani, K.I., 1984. Distribution of directional-data and fabric tensors. International Journal of Engineering Science 22, 149–164.

Laursen, T.A., 2002. Computational Contact and Impact Mechanics. Springer, New York.

Longuet-Higgins, M.S., 1957a. The statistical analysis of a random, moving surface. Philosophical Transactions of the Royal Society of London. Series A-Mathematical and Physical Sciences 249, 321–387.

Longuet-Higgins, M.S., 1957b. Statistical properties of an isotropic random surface. Philosophical Transactions of the Royal Society of London. Series A-Mathematical and Physical Sciences 250, 157–174.

Majumdar, A., Bhushan, B., 1990. Role of fractal geometry in roughness characterization and contact mechanics of surfaces. Journal of Tribology-Transactions of the Asme 112, 205–216.

Mccool, J.I., Gassel, S.S., 1981. The contact of two surfaces having anisotropic roughness geometry, Energy technology, Special Publication. American Society of Lubrication Engineers, New York, pp. 29–38.

Mindlin, R.D., 1949. Compliance of elastic bodies in contact. Journal of Applied Mechanics-Transactions of the Asme 16, 259–268.

Mindlin, R.D., Deresiewicz, H., 1953. Elastic spheres in contact under varying oblique forces. Journal of Applied Mechanics-Transactions of the Asme 20, 327–344.

Misra, A., 1997. Mechanistic model for contact between rough surfaces. Journal of Engineering Mechanics-Asce 123, 475–484.

Misra, A., 1999. Micromechanical model for anisotropic rock joints. Journal of Geophysical Research-Solid Earth 104, 23175–23187.

Misra, A., 2002. Effect of asperity damage on shear behavior of single fracture. Engineering Fracture Mechanics 69, 1997–2014.

Misra, A., Huang, S., 2009. Micromechanics based stress–displacement relationships of rough contacts: Numerical implementation under combined normal and shear loading. Cmes-Computer Modeling in Engineering & Sciences 52, 197–215.

Nayak, P.R., 1971. Random process model of rough surfaces. Journal of Lubrication Technology 93, 398–407.

Persson, B.N.J., Albohr, O., Tartaglino, U., Volokitin, A.I., Tosatti, E., 2005. On the nature of surface roughness with application to contact mechanics, sealing, rubber friction and adhesion. Journal of Physics-Condensed Matter 17, R1–R62.

Wriggers, P., 2006. Computational Contact Mechanics, 2nd ed. Springer, Berlin; New York.

Xia, C.C., Yue, Z.Q., Tham, L.G., Lee, C.F., Sun, Z.Q., 2003. Quantifying topography and closure deformation of rock joints. International Journal of Rock Mechanics and Mining Sciences 40, 197–220.

Yang, J., Komvopoulos, K., 2005. A mechanics approach to static friction of elastic-plastic fractal surfaces. Journal of Tribology-Transactions of the Asme 127, 315–324.

Yoshioka, N., 1994. Elastic behavior of contacting surfaces under normal loads – a computer-simulation using 3-Dimensional surface topographies. Journal of Geophysical Research-Solid Earth 99, 15549–15560.

Yoshioka, N., Scholz, C.H., 1989a. Elastic properties of contacting surfaces under normal and shear loads. 1. Theory. Journal of Geophysical Research-Solid Earth and Planets 94, 17681–17690.

Yoshioka, N., Scholz, C.H., 1989b. Elastic properties of contacting surfaces under normal and shear loads. 2. Comparison of theory with experiment. Journal of Geophysical Research-Solid Earth and Planets 94, 17691–17700.

Zavarise, G., Paggi, M., 2008. Reliability of Micromechanical Contact Models: A Still Open Issue. In: Wriggers, P., Laursen, T.A. (Eds.), CISM International Centre for Mechanical Sciences, vol. 498. CISM, Udine, Vienna.